> MS number: JEDS-2023-11-0319-R. FINAL ms. Jan20-24

Effects of Ion Channeling and Co-implants on Ion Ranges and Damage in Si: Studies with PL, SRP, SIMS and MC models

Michael I. Current, Takuya Sakaguchi, Yoji Kawasaki,
Viktor Samu, Anita Pongracz, Luca Sinko, Árpád Kerekes, Zsolt Durkó

***Abstract*— This study uses photoluminescence (PL) and other carrier-recombination sensitive probes in combination with spreading resistance profiling (SRP), SIMS and IMSIL MC-calculations to monitor the ion range and damage levels in highly-channeled and random beam orientation 7.5 MeV B and 10 MeV P and As profiles and various combinations of co-implants with 50 keV Phosphorus implants in Silicon(100). The effects of annealing on the 10 MeV profiles showed the strong shifts in PL data from implant damage in the as-implanted and annealed samples. Curious "intermittencies" were seen in the PL signals from MeV implant defect centers.**

***Index Terms*—Ion channeling, photoluminescence,** secondary ion mass spectroscopy, spreading resistance profiling, Monte Carlo ion range profiles.

I. INTRODUCTION

Ion implantation of dopants in Si has been used at the predominant form of formation of junctions in transistors for nearly half a century. Despite this long time span and the recent addition of many non-dopant, "materials modification" implants, which now comprise the majority of implants steps in a modern IC process, detailed studies of dopant ranges and effects of implant damage on leakage currents are still relevant, especially as transistors take on new geometrical forms and for new applications beyond logic and memory functions, such as deep photodiode wells in high-sensitivity optical sensors.

In this report we focus on the use of carrier-recombination metrologies, primarily PL, to probe the effects of implant and anneal conditions on leakage current fundamentals. This study follows a line of earlier reports on studies of effects of channeling on MeV implants [1- 3] and many studies of C co-implants with B and P implants [4,5]. See Table 1 for details of the co-implants; ion combinations, ion energies, doses and beam currents and post-implant anneal temperatures.

This work is an expanded version of a paper first presented at the 21st International workshop on Junction Technology (IWJT) at Kyoto University on June 8-9, 2023. This is a collaborative work, with implants done at Sumitomo Implant Technology (SMIT) in Eihime, Shikoku, Japan and most measurements done at SemiLab, Budapest, Hungary. The coordination of the project and most of the reporting was done by the first author. The first and corresponding author is an independent consultant in San Jose, CA USA; Michael Current, email currentsci@aol.com. The second and third authors are with SMIT (emails: yoji.kawasaki@shi-g.com, takuya.sakaguchi@shi-g.com). The fourth through eighth authors are at SemiLab (emails: viktor.samu@semilab.hu, anita.pongracz@semilab.hu, luka.sinko@semilab.hu, arpad.kerekes@semilab.hu,).

II. EXPERIMENTAL DETAILS: IMPLANTS

The high-energy implants were done with a SMIT SS-UHE implanter for 7.5 MeV B and 10 MeV P and As ions at a dose of 3e12 B/cm^2 for the B implants and 5e12 ions/cm^2 for the P and As implants. The beam-wafer incidence angles for these implanters were either "random", with a wafer tilt of 7^o and twist of 23^o, or highly-channeled along the axial channel direction normal to the wafer surface. The SS-UHE implanter provides a beam-wafer angle accuracy of within 0.025^o [6]. The channeled implants were done with wafers cut from the same Si boule with pre-implant characterization of the detailed Si axial tilt.

The co-implant studies with Phosphorus and Carbon ions were done with a combination of SMIT SAion and S-UHE tools with "random" (7/23) beam incidence angles**.** In addition, a series of "random" beam orientation P implants at various doses and ion energies ranging from 10 keV to 1 MeV were tested with PL and SRP to examine the systematic variations in the data.

Table 1: Implants & anneals for P & C co-implants.

Process	Ion	Energy (kev)	Dose (Ions/cm^2)	Ibeam (mA)	Anneal (C)
Dose-anneal	P	50	3e14	1	850
Dose-anneal	P	50	2e14	1	850
Dose-anneal	P	50	1e14	1	850
Dose-anneal	P	50	3e13	1	850
Dose-anneal	P	50	1e14	1	1000
Dose-anneal	P	50	3e14	1	1000
Beam Power	P	150	1e114	7	850
P/C implants	C-P-P	20-50-10	8e13-1e14-1e14	2-1-2.9	850
P/C implants	C-P-P	20-50-10	8e13-1e14-1e14	2-1-2.9	1000
P/P implants	P	50-10	1e14	1-2.9	850
P/P implants	P	50-10	1e14	1-2.9	1000

Note: Anneals were for 30 s in an N_2 ambient.

III. Experimental Details: Measurements

The principle measurement techniques used in this study are: Secondary Ion Mass Spectroscopy (SIMS) and Spreading Resistance Profiling (SRP) for depth profiles of implanted atoms and active carriers and Photoluminescence (PL) and other carrier-recombination related tools, Junction Photovoltage (JPV) and Photo-Modulated Photoreflectance (PMR). A Monte-Carlo ion transport and damage code, IMSIL [7,8], was used to calculate ion ranges and recoil damage profiles for selected random and channeled implants.

PL measurements were done with a SemiLab EnVision photoluminescence tool in the "MicroPL" mode, using a 523 nm laser probe beam with an imaging field of view of 175x140 µm. PL signals from phonon-assisted carrier recombination transitions at wavelengths at ≈1.1 µm and transitions via in-gap defect sites, at wavelengths of 1.3 µm and greater were collected with the use of band pass filters for the two recombination modes. See Fig.1 for Si in-gap phonons and recombination /generations centers and related PL signal wavelenths.

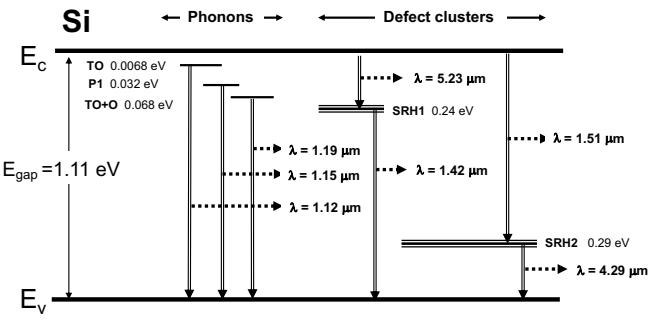

Fig. 1. Principal in-gap state energies and transition wavelengths for carrier recombination paths in Si. The 3 phonon states are within 0.07 eV of the conduction band (E_c). The 2 defect related sites (Shockley-Reid-Hall recombination centers) are within ≈0.25 eV of either the conduction or valance band edges.

IV. Results

A. High Energy Channeling

Stopping Powers

One can start a consideration of the effects of beam incidence along major channeling orientations in crystal targets by identifying channeling conditions as resulting in a significant reduction in nuclear stopping effects from collisions between the incoming fast ion and the atom core electrons in the target. For the common dopants in Si at energies of 7.5 and 10 MeV, the major component in ion stopping is from electronic stopping from ion collisions with loosely bound electrons in outer shells of target atoms and electrons residing in the channeling pathways.

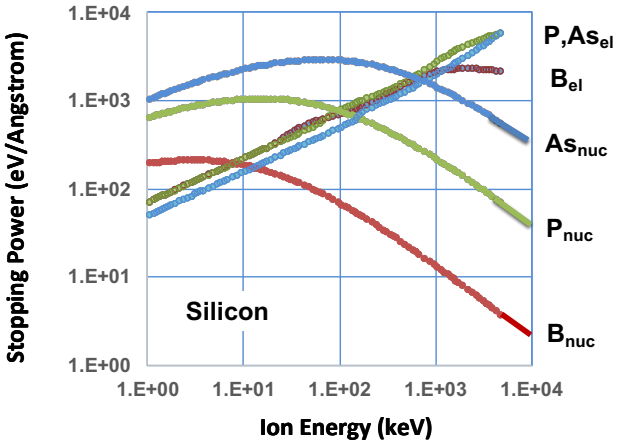

Fig. 2. Electronic and nuclear stopping powers for B, P and As dopants in Si. The stopping powers were calculated by SRIM [6}.

Range and Recoils

Ion ranges for random and channeled beam ordinations for 7.5 MeV B and 10 MeV P and As are shown in Figs. 3 to 5, measured by SIMS and compared to calculations with IMSIL.

The IMSIL calculations were done with a nominal beam divergence of 0.1 degrees.

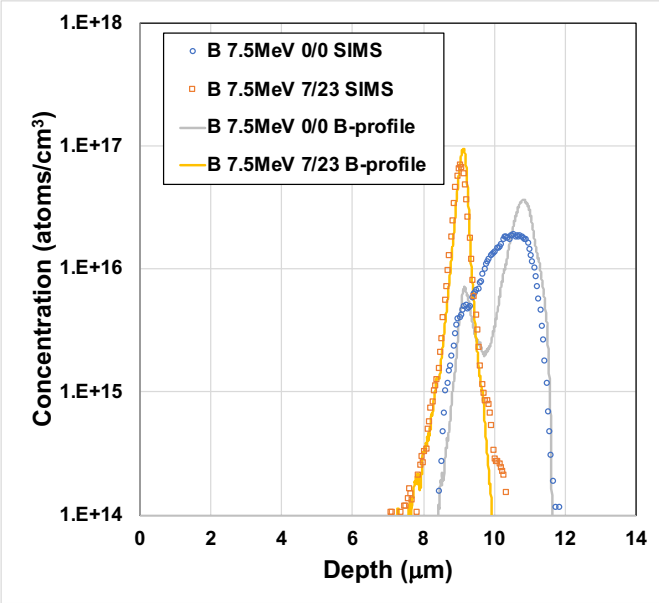

Fig.3. B profiles for random and channeled beam incidence angles for 7.5 MeV B at a dose of 3e12 B/cm^2.

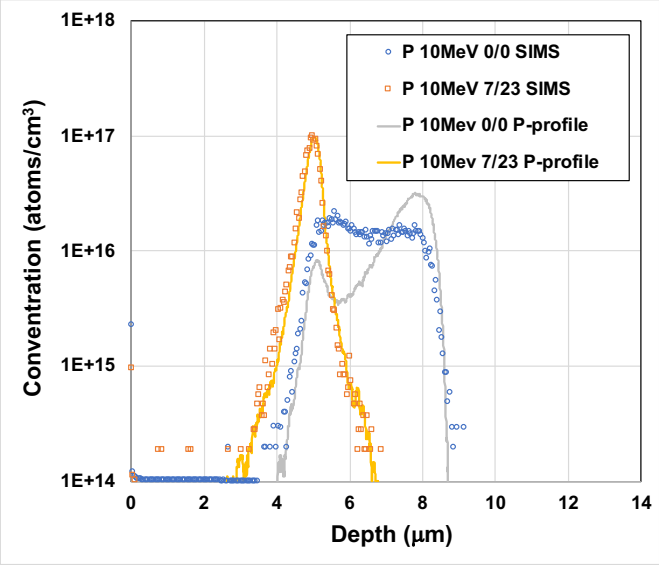

Fig. 4. P profiles for random and channeled beam incidence angles for 10 MeV P at a dose of 5e12 P/cm^2.

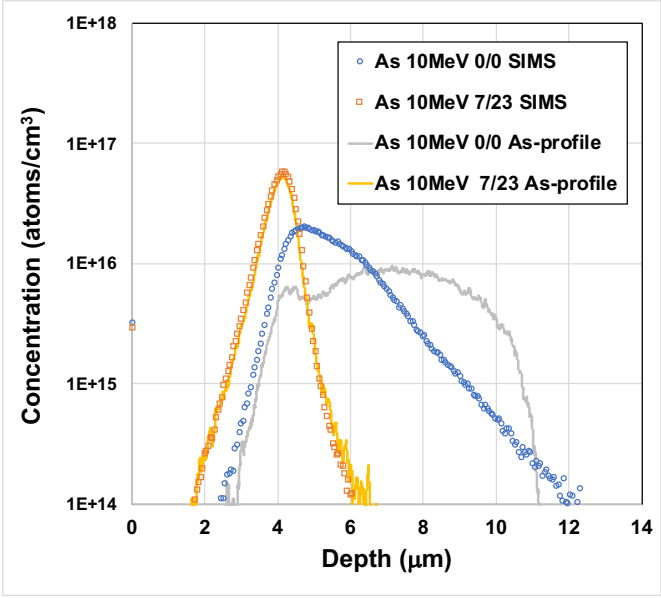

Fig. 5. As profiles for random and channeled beam incidence angles for 10 MeV As at a dose of 5e12 As/cm^2.

Note that the SIMS measured atomic profiles in Figs. 3-5 are closely described by IMSIL calculations for the "random" beam incidence and in only qualitatively agreement for the channeled profiles. Among the many factors that can influence the depth and shape of channeled profiles, beam-wafer alignment, wafer temperature and beam divergence were studied in an earlier paper [1]. Closer agreement between channeled SIMS and IMSIL profiles can be expected with additional refinement of electronic stopping powers for channeled trajectories beyond the work described in [9].

The profiles of Si recoils calculated by IMSIL shown in Fig. 6 give a description of the defect distributions for the as-implanted, primary state of damage for the 3 dopant ions in this study. As one expects from the wide range of nuclear stopping powers in the region of 10 MeV ions, see Fig. 2, the number of Si recoils generated also spans multiple orders of magnitude, with 10 MeV As creating ≈2.2e23 Si recoils/cm^3 for a dose of 5e12 As/cm^2 for a random incidence beam, as tabulated in Table 2. A corresponding random incidence B beam at 7.5 MeV and a dose of 3e12 B/cm^2 results in ≈2e21 Si recoils/cm^3.

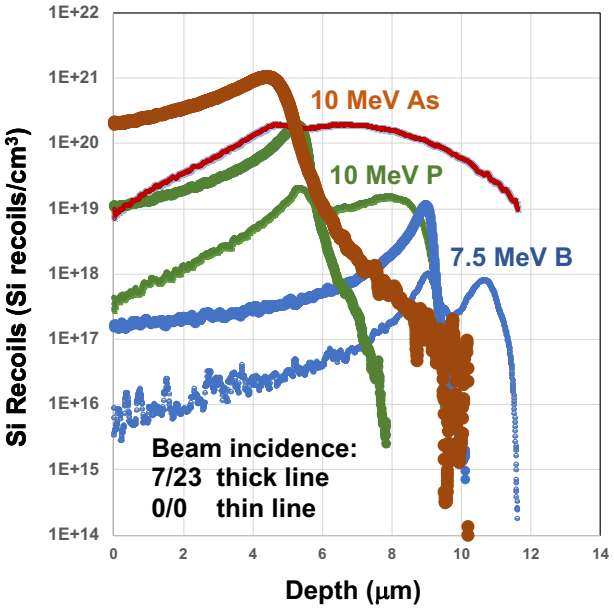

Fig. 6. Si recoil profiles calculated by IMSIL for random and channeled B, P and As ions.

As expected, channeled profiles result in markedly deeper distributions of recoils and lower total generated recoils, see Table 2. Although the number of recoils created by 7.5 MeV B ions is lower than for the heavier ions, the effect of channeled conditions on the total number of recoils created is larger, with an over 80% reduction on Si recoils compared to the random incidence conditions. In comparison, for 10 MeV As, while the atom and recoils distribution depths double with channeling conditions, the total number of recoils is reduced by only ≈15%.

Table 2: Si recoils for Random & Channeled Profiles.

Implantation conditions	Random (7/23) (Si recoils/cm3)	Channeled (0/0) (Si recoils/cm3)	Recoil Ratio (Channeled/ Random)
7.5 MeV B, 3e12 B/cm2	1.93E+21	3.45E+20	0.178
10 MeV P, 5e12 P/cm2	5.27E+22	1.22E+22	0.231
10 MeV As, 5e12 As/cm2	2.24E+23	1.90E+23	0.848

Photoluminescence

The PL images (Fig. 7) for radiation wavelengths >1.3 μm for as-implanted samples were often saturated with overlapping defects and the annealed images showed small numbers of resolved individual radiation sites, making quantitative estimates difficult.

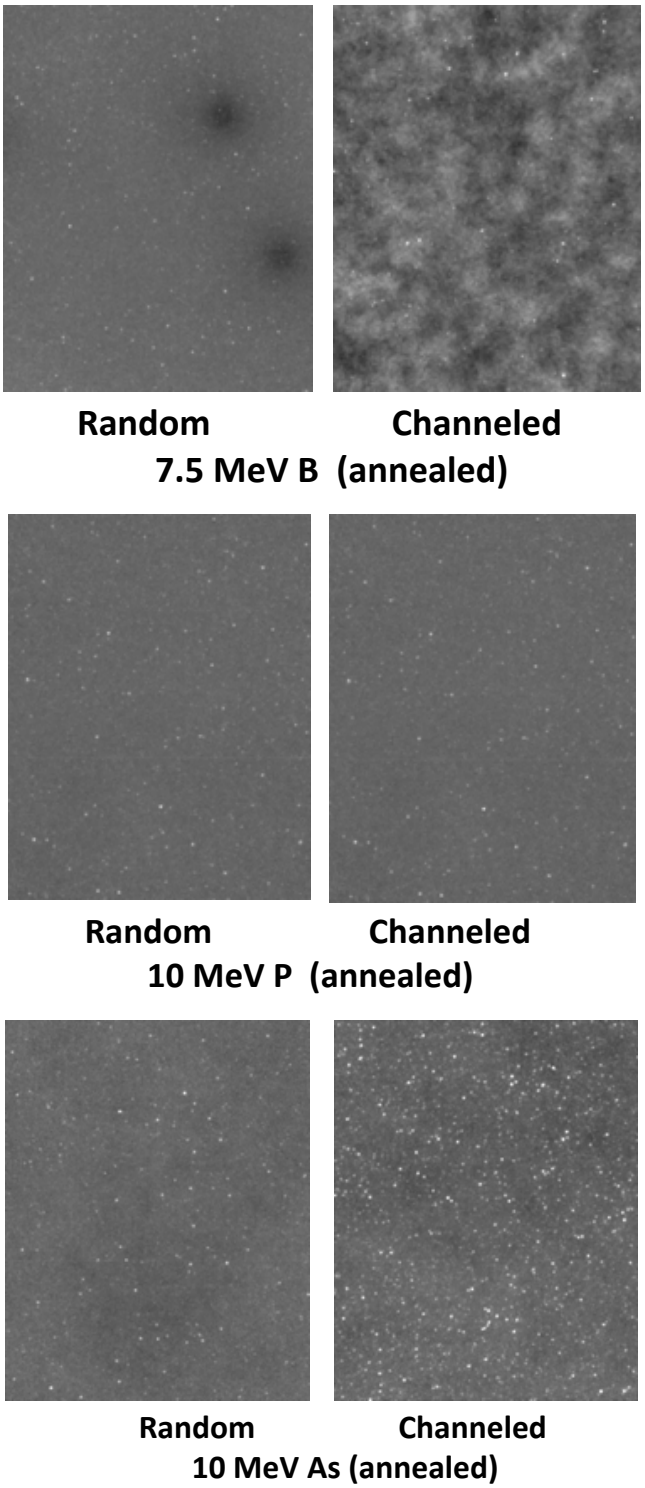

Fig. 7. PL images for random and channeled B, P and As ions after annealing at 950 C/ 3 min/ N_2 ambient, imaged over a field of view of view of 175x140 um.

Quantitative PL data was obtained by comparing the total radiated power from carrier recombination via the phonon-assisted, band-to-band direct channel (at λ ≈ 1.1 μm) and the SRH defect-site-assisted channels (at λ >1.3 μm). If one normalizes the signal from the SRH-related transitions, S^{PL}_{SRH}, by the band-to-band, phonon-assisted radiation power, S^{PL}_{BB},

and assumes that each defect center emits the same PL radiation power, the "Normalized Defect-related PL" = NDPL is:

$$[\ \text{NDPL}\ ] = [\ S^{PL}_{SRH} / S^{PL}_{BB}\ ] \approx n_{SRH} \qquad (1)$$

where n_{SRH} is the number of defect sites contributing to the long-wavelength (at $\lambda > 1.3$ μm) PL signal. This balances out effects from variations in initial carrier creation rates due to variable probe laser beam power and reflection from the sample surfaces.

The NDPL signal trends are determined by the nature, number and distribution of radiative defect sites. For as-implanted profiles, the defect distribution extends over the entire recoil range (Fig. 6) and consist of many isolated vacancy-interstitial pairs (especially for lighter mass ion impacts) and relatively few extended defects. For as-implanted profiles, the NDPL signal is generally strong and is highly sensitive to the total depth of the defect distribution (Fig. 8), with the channeled profiles giving higher signals than the random incidence profiles for each on type and the channeled 7.5 MeV B implant giving the highest NDPL signal.

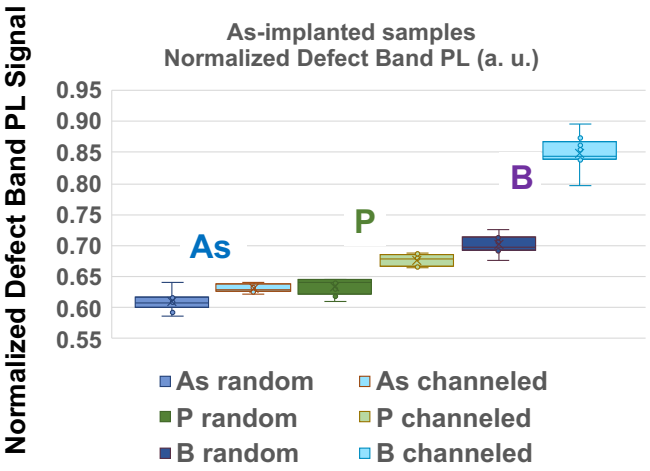

Fig. 8. Normalized defect-related PL signals, [NDPL], for as-implanted B, P and As profiles.

After an anneal at 950 C/ 3 min/ N_2 ambient, the vast majority (>99%) of isolated vacancy-interstitial pairs have recombined and the remaining defects have diffused and formed into extended clusters, <311> rods, dislocation loops, etc. After thermal annealing, the NDPL signal trend reflects the number and luminesce of the residual defect forms. In this case, the overall NDPL signal level is much lower than the as-implants cases and the strongest NDPL signal is from the random incidence As implanted sample, with the highest density of initial defect recoils, and the B implanted samples giving NDPL signals at the noise level. See Fig. 9.

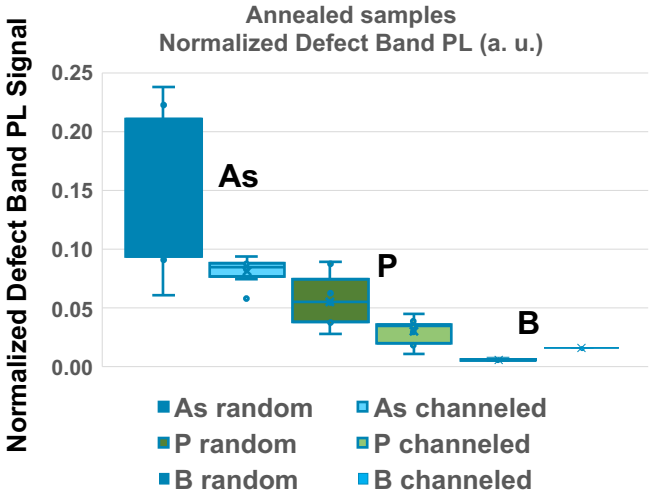

Fig. 9. Normalized defect-related PL signals, [NDPL], for B, P and As profiles after annealing at 950 C/ 3 min/ N_2 ambient.

B. Co-implants with 50 keV P

The samples implanted with 50 keV P and various co-implants, see Table 1, were characterized primarily with PL and SRP tools. A partial summary of results is shown in Table 3. SRP x_j is the electrical junction depth and n(0) is the concentration of carriers at the sample surface.

Table 3: PL and SRP data from 50keV Phos and co-implants.

Implants & Anneals	Total P Dose (P/cm2)	PL Average	SRP Xj (um)	SRP n(0) (n/cm2)
50kV P, 3e14, 1mA, 850C/30s/N2	3.E+14	2035.98	0.25	2.20E+19
50kV P, 2e14, 1mA, 850C/30s/N2	2.E+14	2071.27	0.29	1.10E+19
50kV P, 1e14, 1mA, 850C/30s/N2	1.E+14	851.41	0.18	5.20E+18
50kV P, 3e13, 1mA, 850C/30s/N2	3.E+13	382.09	0.23	1.78E+18
50kV P, 1e14, 1mA, 1000C/30s/N2	1.E+14	396.59	0.14	1.22E+19
50kV P, 3e14, 1mA, 1000C/30s/N2	3.E+14	1218.26	0.25	1.66E+19
150kV P, 1e14, 7 mA, 850C/30s/N2	1.E+14	3635.51	0.49	1.28E+18
20kV C, 8e13, 2 mA: 50kV P, 1e14, 1mA: 10kV P, 1e14, 2.9 mA; 850C/30s/N2	2.E+14	1256.73	0.24	1.32E+19
20kV C, 8e13, 2 mA: 50kV P, 1e14, 1mA: 10kV P, 1e14, 2.9 mA; 1000C/30s/N2	2.E+14	625.75	0.31	8.47E+18
50kV P, 1e14, 1mA: 10kV P, 1e14, 2.9 mA, 850C/30s/N2	2.E+14	1513.19	0.35	5.58E+18
50kV P, 1e14, 1mA: 10kV P, 1e14, 2.9 mA 1000C/30s/N2	2.E+14	397.93	0.28	1.03E+19

All SRP samples were profiled with 10 probe path runs per sample with standard profile smoothing routines. The SRP carrier profiles were compared to atomic profiles from IMSIL and selectively with SIMS. An example an SRP and IMSIL comparison is shown in Fig. 10.

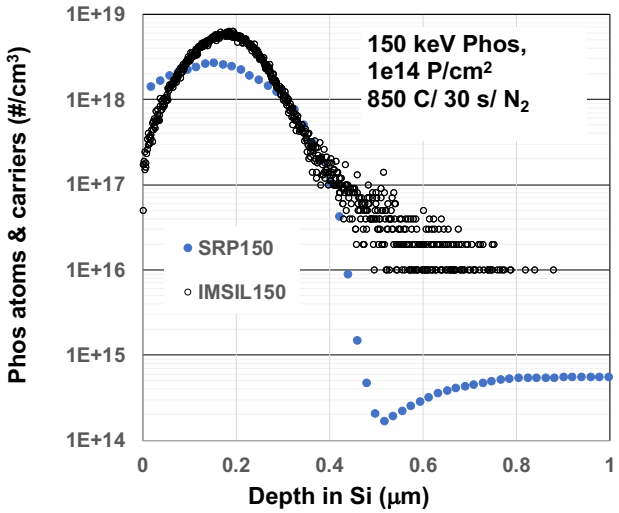

Fig. 10. SRP data and IMSIL calculation for 150 keV P implants after anneal at 850 C/ 30s/ N_2.

Occasionally surprising differences were seen between the active carrier (SRP) and atomic profiles (SIMS & IMSIL), as in the example in Fig. 11 for 50 keV P annealed at 850 and 1000 C, showing low carrier activation in the deeper portions of the profiles.

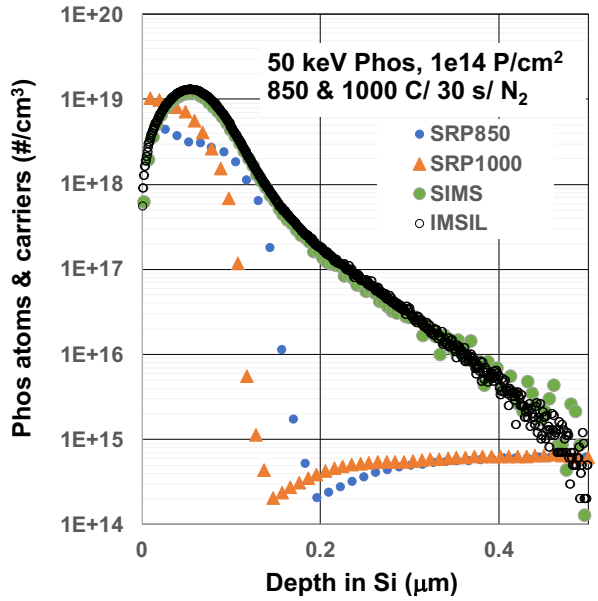

Figure 11. SRP (active carriers) and atomic profiles from SIMS and IMSIL calculation for 50 keV P implants after anneal at 850 C & 1000C / 30s/ N_2, showing poor carrier activation in the deeper portion of the profile.

The co-implants with 20 keV C and annealed at 850 C showed expected effects in PL and SRP data, with lower PL signals (fewer extended defects) and shallower junction depths compared to the dual-P implants without the C co-implant. Annealing at 1000 C generally washed out the effects of the C co-implant.

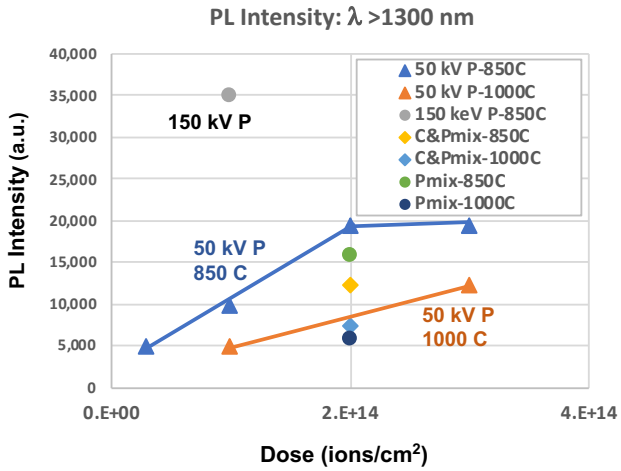

Fig. 12. PL data for defect-related radiation from 50 keV P implants with various P and C co-implants annealed at 850 or 1000 C. Note the higher defect related PL signal for a 150 keV P implant annealed at 850 C.

For the co-implants of 10 and 50 keV P, with PL data shown in Fig. 12, the addition of 20 keV C implants produced an increase in defect sites visible in xTEM images after anneals at 850 C (compare Figs. 13 and 14) even though the radiative defect signals in PL were reduced. Anneals at 1000 C reduced the Pl signals and xTEM visible defects, with or without 20 keV C implants. Illustrating the complexity of these defect effects.

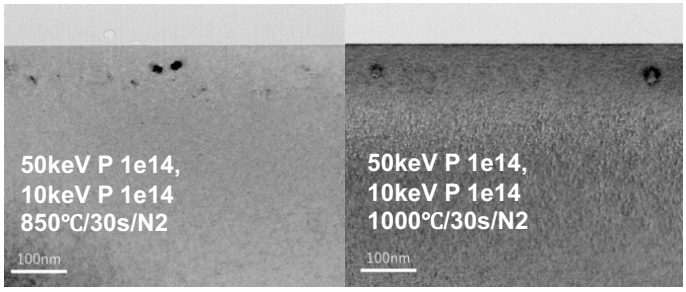

Fig 13. xTEM images of visible defects for co-implants of 10 and 50 keV P after anneals at 850 C (left) and 1000 C (right).

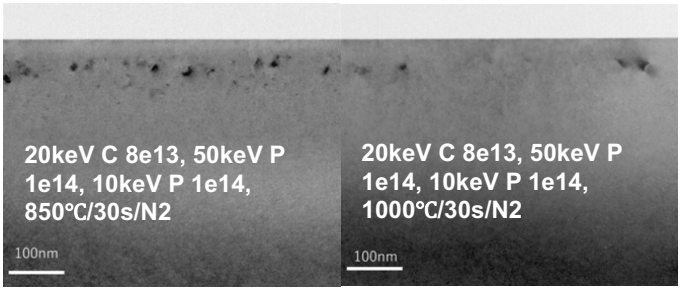

Fig. 14. xTEM images of visible defects after addition of 20 keV C implants to co-implants of 10 and 50 keV P after anneals at 850 C (left) and 1000 C (right).

C. 10 keV to 1 MeV P implants

Additional P implants, with ion energies for 10 keV to 1 MeV were studied with PL and SRP methods. See Table 4 for implant conditions and selected results.

Table 4. 10 keV to 1 MeV Phos implants and data

	Energy (keV)	Dose (ions/cm2)	Beam current (mA)	Sample Set	Slot Number	<X> (um)	Xj (um)	Xj variation (%)	1300LP NDPL
Deep Phos	1000	3.E+13	0.3	2	23	1.08	1.60	0.20	405.0
		1.E+14			24		1.75	0.37	533.9
		3.E+14			25		1.87	0.63	557.6
Mid-E Phos	500	1.E+14	0.3	2	21	0.60	1.34	0.34	381.6
		3.E+14			22		1.29	0.35	408.0
Low-E Phos	150	1.E+14	0.1	2	19	0.20	0.56	0.27	194.2
		3.E+14			20		0.52	0.98	230.8
Low-E Phos	150	1.E+14	1.0	2	17	0.20	0.51	0.57	153.2
		3.E+14			18		0.43	0.41	168.4
Very Low-E Phos	10	1.E+14	2.9	3	3	0.02	0.11	2.17	50.4
		3.E+14			4		0.14	0.92	28.8

Notes on Table 4. The implants were done with a "random" (non-channeled) beam orientation, tilt: 7°, twist: 23°. All samples were annealed before analysis: 850 C/ 30s/N_2 ambient. The ion mean range, <X> was calculated with SRIM. a MC simulation. The electrical junction depth, Xj, was measured from SRP profiles with a variation from 10 SRP profile measurements per case. The normalized Defect-related PL signal (NDPL) was collected with a band pass filter for PL light with a wavelength greater than 1300 um.

The SRP profiles showed a strong dependence on ion energy, as expected, see Fig. 15.

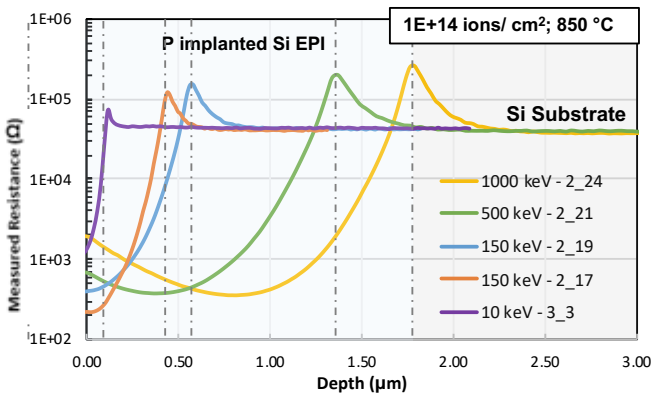

Fig. 15. Spreading resistance profiles for 10, 150, 500 and 1,000 keV P implants into Si at a dose of 1e14 P/cm^2 after an activation anneal at 850 C.

Note in Fig. 15 the effect of ion beam current on the SRP electrical junctions for 150 keV P, with the measured Xj for a beam current of 1mA (sample 2-17) being measurably shallower than the profile implanted with a beam current of 100 uA (sample 2-19, consistent with the higher damage accumulation rates with the higher beam current, reducing the effects of indirect channeling on the P profiles [10].

Increased in the ion dose at a constant ion energy resulted in deeper P diffusion during the 850 C activation anneal and deeper measured electrical junction depths, see Fig. 16.

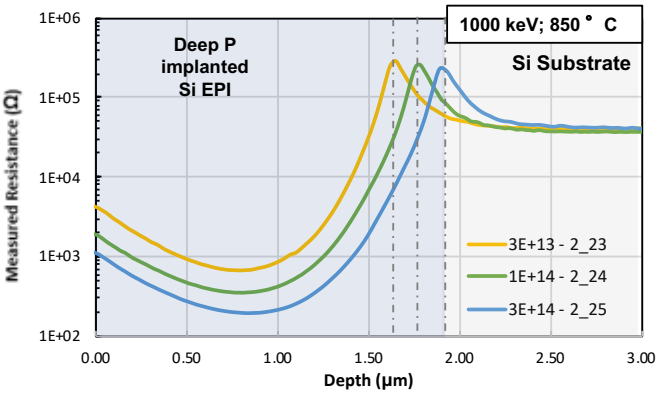

Fig. 16. Spreading resistance profiles for 1,000 keV P implants into Si at doses of 3e13, 1e14 and 3e14 P/cm^2 after an activation anneal at 850 C.

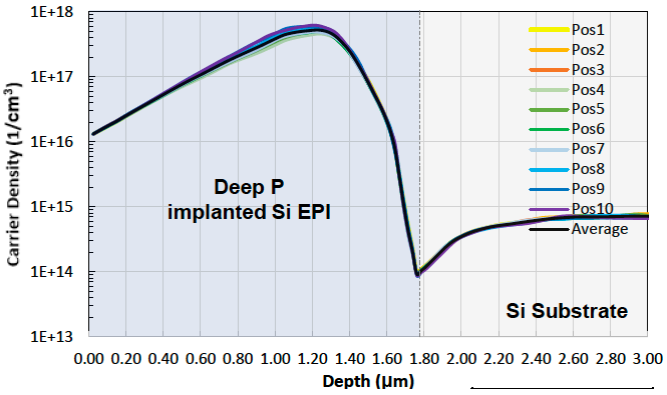

Fig. 17. Carrier concentration profile calculated for spreading resistance data for the case of 1,000 keV P at a dose of 1e14 P/cm^2 after an activation anneal at 850 C.

In Fig. 17, slight variations in the calculated carrier density are visible near peak of the dopant concentration, with a variation in the measured electrical junction depth at 0.37% (for a 10 SRP profile data set) for this case.

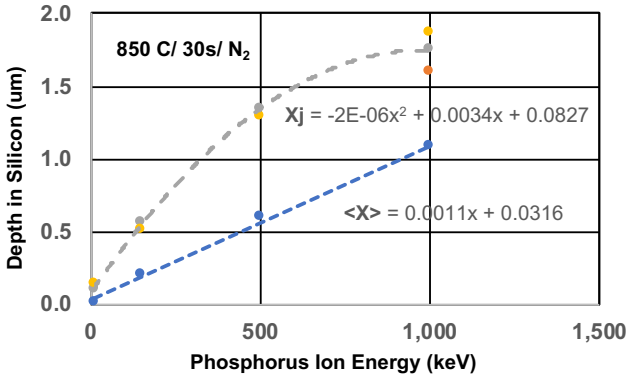

Fig. 18. Electrical junction depths, Xj, measured by SRP for Phos implants for 10 to 1,000 keV P implants into Si after an activation anneal at 850 C. Also shown are the ion mean range values, <X>, calculated from SRIM.

Note in Fig. 18 the 3 Xj values plotted for 1000 keV P, corresponding to the spreading resistance profiles shown in Fig. 16, showing the combined effects of ion energy, ion dose and diffusion during activation anneals on the measured electrical junction depth.

The Normalized Defect-related PL (NDPL) signals after thermal annealing respond to the surviving recombination centers after the majority of the implant damage has annealed out (see earlier discussion of photoluminescence).

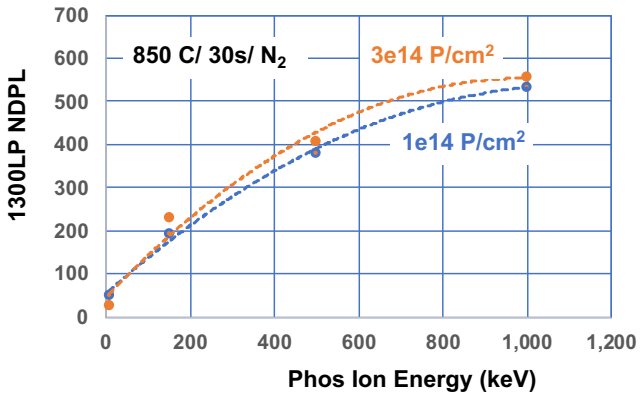

Fig. 19. Normalized defect-related PL signals (NDPL) for Phos implants at 10, 150, 500 and 1,000 keV P at doses of 1e14 and 3e14 P/cm^2 after an activation anneal at 850 C for 30 s.

D. Observations of PL site radiation "intermittency"

When observing the micro-PL images for 7.5 and 10 MeV dopants, see Fig. 7, it was noticed that individual radiative sites would "blink" on and off when observed for 10s of minutes under constant PL probe beam powers. Observation of individual radiative sites over the course of ≈40 min showed an apparently random "intermittency" from many sites, see an example in Fig. 15, showing 3 levels of radiative luminosity. For the optics used in the PL tool, the spatial resolution was ≈1 um for imaging individual radiative recombination centers.

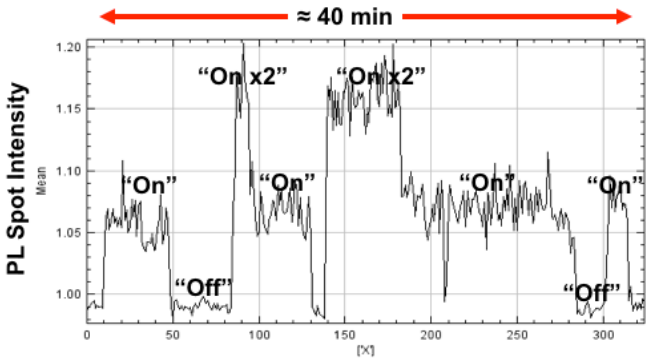

Fig. 20. PL defect signals from a *single* radiation center over a time sample of ≈40 min, showing 3 levels of luminosity, indicating changes of state over time at a single defect site as carriers are recombined.

Similar radiative effects have been observed in PL data from arrays of quantum dots and other systems [11]. These PL intermittencies suggest a link to Jahn-Teller distortions, first described in 1937 discussing the degeneracy and stability of non-linear molecular systems [12]. This suggests that understanding these PL effects with detailed molecular vibrational modeling of recombination events at defects sites could lead to the use of PL measurements as a new form of defect spectroscopy.

V. Summary

Radiative emission from carrier recombination in Si, observed as photoluminescence, provides a powerful analytical tool for study of as-implanted and annealed residual damage in ion implanted Si when coupled with measurements of atomic (SIMS) and carrier (SRP) profiles combined with MC calculations of atom and recoil profiles (IMSIL), as shown in these studies.

ACKNOWLEDGMENT

We acknowledge the assistance of Philip Mauger at Nanostructures, Sunnyvale, CA for some of the anneals used in this work, the guidance of Gerhard Hobler at TU Wein with the use of IMSIL and the support and useful discussions with Tom Bergman, a consultant with Sumitomo Heavy Industries Implant Technologies, throughout the course of this work.

REFERENCES

[1] M.I. Current, G. Hobler, Y. Kawasaki, M. Sugitani, "Channeled MeV B, P and As Profiles in Si(100): Monte-Carlo Models and SIMS"; *Proc. IIT18.* ISBN 978-1-5386-6827-6 (2019) pp. 251-254.

[2] M.I. Current, G. Hobler, Y. Kawasaki, "Aspects of Highly-channeled MeV Implants of Dopants in Si(100)", *Proc. International Workshop on Junction Technology (IWJT19)*, Uji, Japan, June 6-7, 2019.

[3] M.I. Current, Y. Kawasaki, T. Sakaguchi, A. Pongrácz, V. Samu, "Profiles and defects in highly-channeled and random beam orientation MeV dopant implants in Si(100)", IIT22, *MRS Advances (2022) 7:1454–1458*, doi.org/10.1557/s43580-022-00481-2.

[4] B. J. Pawlak, T. Janssens, B. Brijs, W. Vandervorst, E. J. H. Collart, S. B. Felch, and N. E. B. Cowern, "Effect of amorphization and carbon co-doping on activation and diffusion of boron in silicon", *Appl. Phys. Lett*., **89** (2006) p. 062110.

[5] B. J. Pawlak, R. Duffy, T. Janssens, W. Vandervorst, S. B. Felch, E. J. H. Collart, and N. E. B. Cowern, "Suppression of phosphorus diffusion by carbon co-implantation", *Appl. Phys. Lett., **89** (2006)* p. 062102.

[6] www.srim.org.

[7] H. Kariya, S. Kawatsu, H. Sasaki, Y. Kimura, N. Ido, Y. Kawasaki, M. Kabasawa, "Precise angle control for channeling using SS-UHE, a single-wafer ultrahigh-energy ion implanter", IIT22, *MRS Advances (2022) 7:1285–1288*, doi.org/10.1557/s43580-022-00490-1.

[8] G. Hobler, "Monte Carlo simulation of two-dimensional implanted dopant distributions at mask edges", *Nucl. Instrum. Meth. B 96* (1995) p.155.

[9] G. Hobler and B. Murthy, "Towards a comprehensive model of electronic stopping in amorphous and crystalline silicon", *Proc IIT2000*, IEEE 00EX432 (2001) pp. 209-212.

[10] K.R.C. Mok et al., "Comprehensive model of damage accumulation in silicon", *J. Appl. Phys. 103* (2008) 014911.

[11] E.A. Riley, C.M. Hess, P.J. Reid, "Photoluminescence intermittency from single quantum dots to organic molecules: Emerging themes", *Int. J. Molecular Sciences 13* (2012) 12487-12518.

[12] H.A Jahn, E. Teller, *Proc. Roy. Soc. London A,* (1937**)**, *161*,220-235. DOI: 10.1098/rspa.1937.0142.